Pressure-induced disordering of site occupation in iron–nickel nitrides

Binbin Wu,[1] [ID] Li Lei,[1,a)] [ID] Feng Zhang,[1] Qiqi Tang,[1] Shan Liu,[1] Meifang Pu,[1] Duanwei He,[1] [ID] Yuanhua Xia,[2] Leiming Fang,[2,a)] [ID] Hiroaki Ohfuji,[3] and Tetsuo Irifune[3] [ID]

AFFILIATIONS

[1]Institute of Atomic and Molecular Physics, Sichuan University, Chengdu 610065, China
[2]Institute of Nuclear Physics and Chemistry, Academy of Engineering Physics, Mianyang 621900, China
[3]Geodynamics Research Center, Ehime University, Matsuyama 790-8577, Japan

[a)]Authors to whom correspondence should be addressed: lei@scu.edu.cn and flmyaya2008@163.com

ABSTRACT

Controlled disordering of substitutional and interstitial site occupation at high pressure can lead to important changes in the structural and physical properties of iron–nickel nitrides. Despite important progress that has been achieved, structural characterization of ternary Fe–Ni–N compounds remains an open problem owing to the considerable technical challenges faced by current synthetic and structural approaches for fabrication of bulk ternary nitrides. Here, iron–nickel nitride samples are synthesized as spherical-like bulk materials through a novel high-pressure solid-state metathesis reaction. By employing a wide array of techniques, namely, neutron powder diffraction, Rietveld refinement methods combined with synchrotron radiation angle-dispersive x-ray diffraction, scanning electron microscopy/energy dispersive x-ray spectroscopy, and transmission electron microscopy, we demonstrate that high-temperature and high-pressure confinement conditions favor substitutional and interstitial site disordering in ternary iron–nickel nitrides. In addition, the effects of interstitial nitrogen atoms and disorderly substituted nickel atoms on the elastic properties of the materials are discussed.

I. INTRODUCTION

Iron and nickel are the most important components of the inner core of the Earth, with recent reports indicating that at 364 GPa and 5000–6000 K, the maximum nitrogen content in the inner core can vary from 2.0 to 3.2 wt. %.[1–5] The study of iron–nickel alloys and iron–nickel nitrides has been an important focus of experimental and computational research over the past few decades.[6–10] Iron–nickel alloys also have considerable potential for materials applications, owing to their high magnetoconductivities and low coefficients of thermal expansion.[11,12] Iron-based nitrides have been considered important candidates for use as corrosion-proof layers on steel and for magnetic data storage systems, thanks to their significant thermal stability and suitable magnetic properties.[13–15] The ordering of substitutional and interstitial site occupation at high pressures can lead to fundamental changes in structural phase relationships and in the properties of iron–nickel nitrides. The structural properties of iron–nickel nitrides are of considerable interest for a wide range of researchers, especially those in materials science, chemistry, physics, and earth science.

In iron-based nitrides, nitrogen atoms enter the lattice to form interstitial solid solutions, such as γ-Fe$_4$N and ε-Fe$_3$N. The crystal structures of γ-Fe$_4$N and ε-Fe$_3$N derive from the face-centered cubic (fcc) γ-Fe structure and the hexagonal close-packed (hcp) ε-Fe structure, respectively.[16,17] In the ideal binary nitride γ-Fe$_4$N (Pm-$3m$), Fe atoms occupy both the Wyckoff $3c$ and $1a$ sites [Fig. 1(a)], but in the case of the ternary nitride γ-Fe$_3$NiN (Pm-$3m$), Fe and Ni atoms occupy the Wyckoff $3c$ and $1a$ sites, respectively,[18,19] with the N atom occupying the $1b$ site [Fig. 1(b)]. In analogy with the aforementioned case, in the iron–nickel alloy γ-FeNi$_3$ (Pm-$3m$), the Fe and Ni atoms tend to occupy the Wyckoff $1a$ and $3c$ sites, respectively, with the interstitial $1b$ site remaining vacant [Fig. 1(c)]. In the standard structure of ε-Fe$_3$N ($P6_3$22), each iron atom at the $6g$ site coordinates with two nearest-neighbor nitrogen atoms at the $2c$ positions [the only available position for N atoms: see Fig. 1(d)]. Interestingly, Leineweber et al.[17] suggested possible occupancy of the $2b$ site by the N atoms together with absence of occupancy for the $2d$ site. This was explained on the basis of N–N repulsive forces as being due to the minimized configurational entropy probed by time-of-flight (TOF) neutron diffraction.[17] Our recent
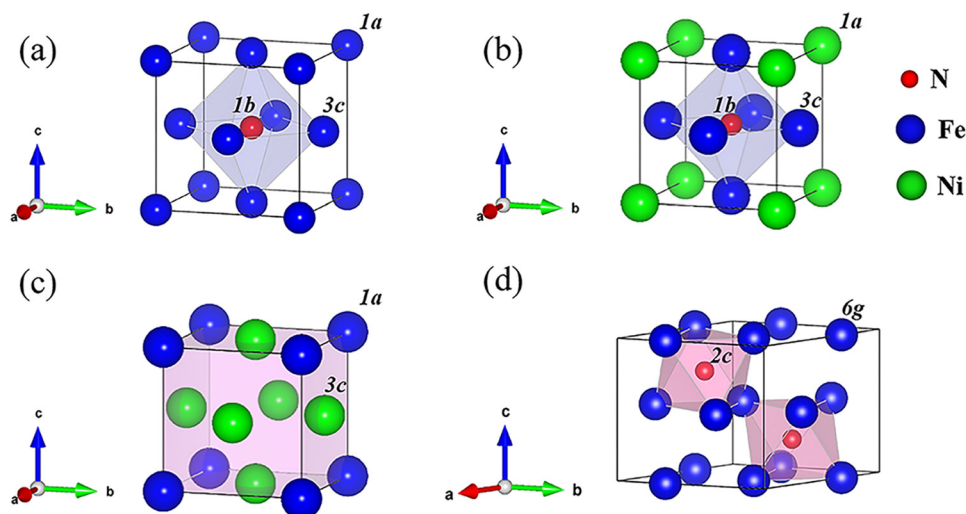
FIG. 1. Ideal crystal structures of (a) γ-Fe$_4$N, (b) γ-Fe$_3$NiN, (c) γ-FeNi$_3$, and (d) ε-Fe$_3$N. The blue and green balls represent Fe and Ni atoms, respectively, and the red ball the N atom.

neutron powder diffraction (NPD) study of nitrogen-rich ε-Fe$_3$N and ε-Fe$_{2.322}$Co$_{0.678}$N$_{0.888}$ nitrides has shown that nitrogen atoms may enter the higher-entropy interstitial 2b and 2d sites, and the Co and Fe atoms could disorderly occupy the cation 6g site at high temperature and high pressure (HTHP).[20] The conditions for the formation of substitutional solid solutions in metals can be described by the Hume-Rothery rules.

The structure and properties of iron-based nitrides can be significantly affected by disordered interstitial N atoms and substitutional Co atoms. To the best of our knowledge, up to now, there have been only a few reports of detailed structural property studies of ternary iron-based nitrides. Despite important progress, the cation occupancy in ternary iron–nickel nitrides at high pressure remains poorly understood. A detailed investigation of the structural properties of iron–nickel nitrides is therefore needed, in order to shed light on the dynamics of cation occupancy at high pressure.

The preparation of metal nitrides is particularly challenging under ambient conditions, owing to difficulties in incorporating nitrogen into the metal lattice, given the thermodynamically disadvantageous conditions under ambient pressure. Instead, a high-pressure enclosing environment is thermodynamically beneficial for both the reactivity of nitrogen and the stability of the nitrides. Bulk single-crystalline ε-Fe$_3$N phases have been synthesized by Niewa et al.[21] using microcrystalline ε-Fe$_3$N$_{1+x}$ as starting material at 15 GPa and 1327 °C. Guo et al.[22] have further shown that Co or Ni atoms can occupy Fe sites in ε-Fe$_2$CoN or ε-Fe$_2$NiN phases, synthesized from mixtures of ζ-Fe$_2$N and Co (or Ni) at 5 GPa and 1200 °C. High-pressure solid-state metathesis (HPSSM) reactions provide a useful synthetic method for fabrication of metal-based nitrides.[20,23] Metal oxides, such as Fe$_2$O$_3$, Co$_2$O$_3$, NiO, LiNiO$_2$, LiGaO$_2$, KGaO$_2$, NaReO$_4$, Na$_2$MoO$_4$, and K$_2$OsO$_4$, are used as precursors in HPSSM reaction routes for the production of spherical bulk iron-based nitride samples, such as ε-Fe$_3$N$_{1+x}$ and γ-Fe$_4$N$_x$.[24–29]
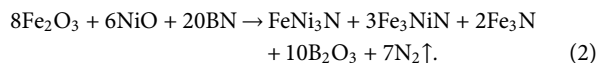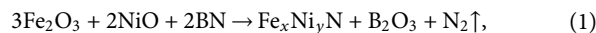
The principal motivation for this study is the synthesis of bulk ternary iron–nickel nitrides under HTHP conditions and further investigation and explanation of the disordering of substitutional and interstitial site occupancy, with the aim of obtaining better understanding of the structural properties of iron–nickel nitrides at high pressure.

II. EXPERIMENTAL DETAILS

A. High-pressure synthesis

Iron–nickel nitrides were synthesized using an HPSSM reaction in which Fe$_2$O$_3$, NiO, and hBN were used as reaction precursors. The reactions are as follows:

$$3\text{Fe}_2\text{O}_3 + 2\text{NiO} + 2\text{BN} \rightarrow \text{Fe}_x\text{Ni}_y\text{N} + \text{B}_2\text{O}_3 + \text{N}_2\uparrow, \qquad (1)$$

$$8\text{Fe}_2\text{O}_3 + 6\text{NiO} + 20\text{BN} \rightarrow \text{FeNi}_3\text{N} + 3\text{Fe}_3\text{NiN} + 2\text{Fe}_3\text{N}$$
$$+ 10\text{B}_2\text{O}_3 + 7\text{N}_2\uparrow. \qquad (2)$$

The nominal composition of the starting mixtures is Fe$_2$O$_3$:NiO: BN = 3:2:2, and x and y can be varied in the ideal reaction (1). Reaction (2) is the actual reaction under the experimental pressure of 5 GPa and for $T \approx 1673$ K. The high-pressure synthesis experiments were performed on a cubic large-volume press (DS6×14 MN, China). The precursors were mixed at different molar ratios and precompacted into a cylinder of radius 4 mm and height 8 mm (in the HPSSM experiments). The sample was sealed in a cylindrical capsule made of hBN and was then packed in a pyrophyllite high-pressure cell. The high-pressure cell was then heated to 1400–1600 °C under 5 GPa pressure held for 5–20 min. The temperature was then reduced, while the pressure was relieved to ambient conditions. The resulting metallic spherical bulk samples of diameter ~5 mm were harvested in the high-pressure cell after the high-pressure synthesis experiments. The byproduct boron oxide (mostly distributed around the sample) could be easily removed by washing.

B. Structural Characterization

The structural properties of the as-synthesized iron–nickel nitride samples were investigated by microfocus x-ray diffraction

(XRD) (Rigaku, RAPIDII-V/DW, Cu $K\alpha$). The quantitative accuracy was estimated to not exceed 0.5%. The elemental distribution of the samples was analyzed by high-angle annular dark field scanning transmission electron microscopy (HAADF-STEM) (JEOL-TEM, Japan). The crystal structure was determined by selected area electron diffraction (SAED). The homogeneity of the iron–nickel nitrides was measured by scanning electron microscopy (JSM-7000F field emission SEM, JEOL), and the elemental composition was determined using energy dispersive x-ray spectroscopy (EDX) (INCA E250, Oxford Instruments). A 5 nm thick osmium coating on the surface of each sample was produced using an osmium coater (Neoc-STB, Meiwafosis Co., Ltd.) before EDX measurement. FeS_2, Ni, and BN were used as the EDX standards for the quantification of Fe, Ni, and N, respectively.[30]

An *in situ* high-pressure synchrotron angle-dispersive x-ray diffraction (ADXRD) study was performed at ambient temperature on a symmetric type of diamond anvil cell (DAC) with 500 μm culet anvils at the 4W2 high-pressure beamline of the Beijing Synchrotron Radiation Facility (BSRF). Each iron–nickel nitride sample together with a small ruby ball of approximately 10 μm was placed in the 120 μm chamber of a rhenium gasket for indentation to a thickness of about 40 μm.

The ruby fluorescence technique was used to calibrate the pressure, while methanol/ethanol 4:1 (by volume) was used as the pressure-transmitting medium.[31] For the ADXRD measurements, a Si (111) monochromator was used to produce synchrotron radiation x rays of wavelength 0.6199 Å. The ADXRD patterns of the samples thus obtained were integrated using FIT2D software.[32,33]

Neutron powder diffraction (NPD) is an effective and exact technique to accurately determine atomic occupancy. In this work, we performed NPD experiments on the iron–nickel nitride samples at room temperature using the Fenghuang neutron diffractometer at the China Mianyang Research Reactor (CMRR) of the Institute of Nuclear Physics and Chemistry, China.[32] The elemental neutron scattering length parameters in the iron–nickel nitride samples are $b(Fe) = 0.954 \times 10^{-12}$ cm, $b(Ni) = 1.031 \times 10^{-12}$ cm, and $b(N) = 0.936 \times 10^{-12}$ cm. A thin-walled copper chamber of diameter 6 mm was used to enclose the iron–nickel nitride samples (each weighing approximately 3 g). The NPD data were collected in the range of $2\theta = 20°–140°$ in steps of $0.1° s^{-1}$ and at a wavelength $\lambda = 1.57$ Å. The sampling time was 10 h, and the neutron flux at the sample position was $2.84 \times 10^6 \, n \, s^{-1} \, cm^{-2}$. The data were refined using FullProf Suite Toolbar version 2.05 Rietveld refinement software.[34] For the refined NPD patterns of the iron–nickel nitrides, the reliability factors were $R_{wp} = 30.2\%$ and $\chi^2 = 2.09$.

III. RESULTS AND DISCUSSION

Owing to the effects of the lower surface energy, the as-synthesized nitride samples from the HPSSM reaction were spherical in shape [Fig. 2(a)]. In the HPSSM reaction, nitrogen degassing leads to formation of abundant cavities inside the iron–nickel nitride samples, as shown in Fig. 2(b). Typical bone-shaped interdendrite phases were also detected, together with elemental segregation [Fig. 2(c)]. This effect is associated with dendritic segregation in nickel-based superalloys, as a side-effect of solidification.[35,36] The different grayscale regions in the SEM image in Fig. 2(d) (marked as A, B, and C) indicate different phases in the sample. In fact, although we

have conducted many high-pressure experiments in which the pressure–temperature–composition–time parameters ($P–T–x–t$) were varied, almost all the successful experiments resulted in multiple-phase products.

The typical result of an HAADF-STEM acquisition is shown in Fig. 3(a), while Fig. 3(b) shows SAED patterns of the iron–nickel nitrides, containing phases A, B, and C corresponding to the three sets of diffraction spots. Figure 3(c) is a schematic diagram of the SAED pattern, with the diffraction spots corresponding to phases A, B, and C in red, blue, and green, respectively. The elemental distributions within different nitride phases was investigated further. Typical elemental maps obtained from STEM-EDX measurements are shown in Figs. 3(d)–3(f). Phase A has the highest Ni and lowest N content, while phase C has the highest Fe and lowest Ni content. An identical conclusion is obtained from a consideration of the dynamics of dendrite segregation.

The elemental composition was determined by EDS, and the outcome of the refined NPD and XRD patterns is shown in Table I. For all three phases, neither NPD nor EDX detected boron and oxygen elements, which is consistent with the results of our previous studies of HPSSM reactions.[20,23–25,37,38] Determination of elemental compositions by different methods can yield different outcomes owing to the working principles of the particular method. For example, EDX determines elements according to their different characteristic x-ray emissions, XRD is based on interactions between x rays and electrons, and NPD is based on neutron and nuclear interactions. The analytical scales also differ between these methods: micro-focused XRD measurements cover a few tens of micrometers, and EDX analysis is effective within the order of a micrometer, while NPD requires a significantly larger sample volume. Therefore, the differences in chemical composition determined by the various
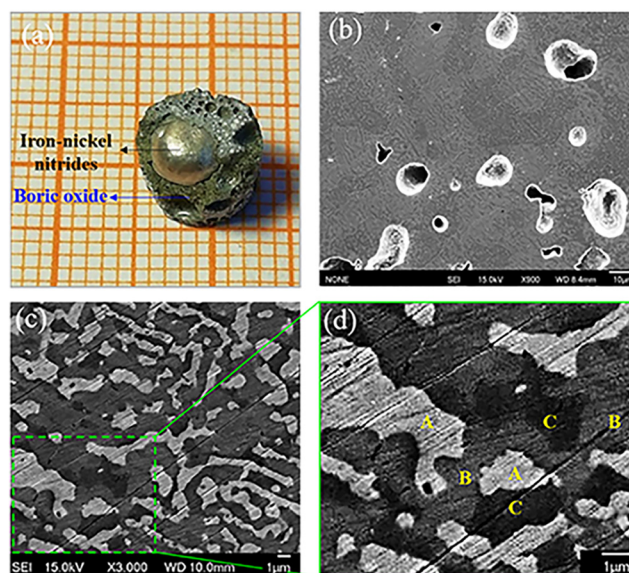
FIG. 2. (a) Typical reaction product from an HPSSM experiments. (b) In the reactions, nitrogen degassing leads to abundant cavities. (c) and (d) SEM images of typical iron-nickel nitride samples.
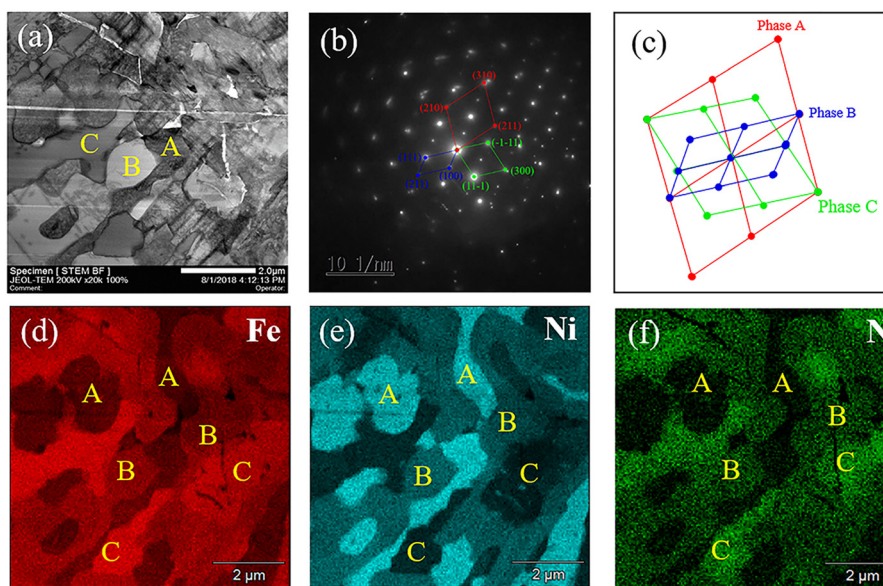
FIG. 3. (a) HAADF-STEM image of an iron–nickel nitride. (b) The corresponding SAED pattern, where the spots corresponding to phases A, B, and C are represented in red, blue, and green, respectively. (c) Schematic diagram of the SAED pattern, with each color corresponding to a crystal structure. (d)–(f) Corresponding STEM-EDX elemental maps showing the distributions of Fe, Ni, and N, respectively, with A, B, and C representing γ-FeNi$_3$-type, γ-Fe$_4$N-type, and ε-Fe$_3$N-type nitrides, respectively.

methods may be caused by the different sizes of the area analyzed. Taking into account that the NPD method is more reliable for samples that contain neighboring elements (such as Fe and Ni) and light elements (such as N), in this work the ratios of atomic composition were determined from the NPD results alone.[39–41]

According to the Hume-Rothery rules, when the difference in atomic size between two elements is greater than 15%, it is difficult for them to form a substitutional solid solution.[40] Owing to the atomic-size difference $\delta_{\{Fe, Ni\}} = 18.25\% > 15\%$, therefore, it is difficult to form pure phases of iron–nickel nitrides by employing Ni as a substitute for Fe. On the other hand, because the mixing enthalpy reflects the atomic binding energy, the mixing enthalpy and atomic-size difference were selected in order to study the law of phase formation of iron–nickel nitrides. The segregation phenomenon can be explained by the enthalpy of mixing between the principal elements. The mixing enthalpies values are as follows: $\Delta H^{mix}_{\{Fe,N\}} = -87$ kJ/mol, $\Delta H^{mix}_{\{Ni,N\}} = -69$ kJ/mol, and $\Delta H^{mix}_{\{Fe,Ni\}} = -2$ kJ/mol.[42] Since Fe shows a higher negative enthalpy when mixed with Ni, it is partially attracted to the dendrite region by the Ni component. By contrast, N exhibits lower negative enthalpy with Fe and Ni, and thus it is repelled from the dendrite region.
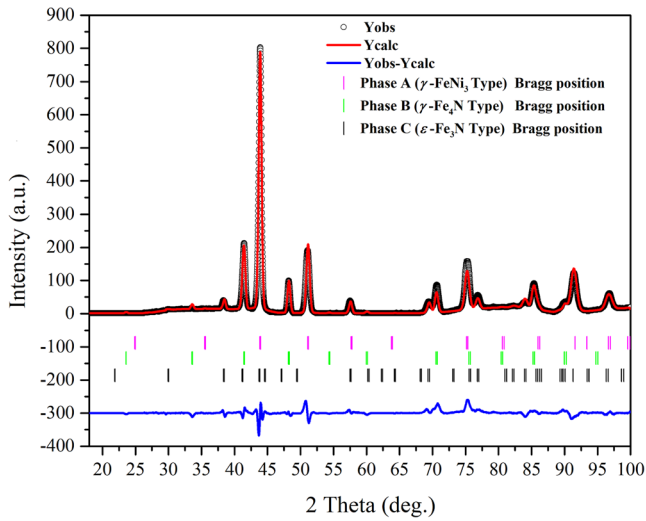
The micro-focused XRD patterns of iron–nickel nitrides collected under ambient conditions (Fig. 4) were analyzed using the Rietveld refinement method. This yielded three nitride phases with reliability factors $R_{wp} = 22.5\%$ and $\chi^2 = 0.74$. The refined lattice constants are listed in Table II, and it can be seen that no obvious lattice distortion was found in the present experiments. According to the structural and compositional analysis, the bone-shaped inter-dendrite phase is mainly of γ-FeNi$_3$ type, which is recorded as phase A, while the dendrite matrix is composed of Fe, Ni, and N, and this is recorded as phase B (γ-Fe$_4$N type) and phase C (ε-Fe$_3$N type). These phases correspond to the areas marked A, B, and C in Fig. 2(d). The existence of three N-bearing compounds was further confirmed by XRD, and this is consistent with our observations from SEM.

To gain a better understanding of the produced materials, the compressibility parameter was investigated. The synchrotron radiation diffraction data indicate that the iron–nickel nitride samples are stable in the pressure range 0–25 GPa (at room temperature). As the pressure is increased, the positions of all the diffraction peaks of the iron–nickel nitrides are found to shift toward larger 2θ values This observation highlights a pressure-induced decrease in the d spacing, and therefore a decrease in the unit-cell volume. The pressure evolution of the unit-cell parameters of phases A, B, and C are shown in Fig. 5. The pressure–volume curves for phases A, B and C were fitted with a third-order Birch–Murnaghan equation of state (EOS)

TABLE I. Elemental compositions of the three phases as determined by EDS, NPD, and XRD.

	Phase A (γ-FeNi$_3$ type)	Phase B (γ-Fe$_4$N type)	Phase C (ε-Fe$_3$N type)
EDS	FeNi$_{2.94}$N$_{0.02}$	Fe$_{2.87}$Ni$_{1.27}$N	Fe$_{2.33}$Ni$_{0.72}$N
XRD	FeNi$_{3.15}$N$_{0.06}$	Fe$_{3.06}$Ni$_{1.02}$N	Fe$_{1.70}$Ni$_{1.29}$N
NPD	FeNi$_{3.21}$N$_{0.08}$	Fe$_{2.94}$Ni$_{1.08}$N	Fe$_{1.58}$Ni$_{1.42}$N

FIG. 4. Rietveld refinement (red line) applied to micro-focused XRD patterns acquired from iron–nickel nitride samples.

FIG. 5. Plots of normalized unit-cell volume vs pressure for iron–nickel nitrides. The inset shows Rietveld refinement patterns from synchrotron radiation ADXRD of iron–nickel-based nitride powder under a pressure of 1.87 GPa.

$$P(V) = \frac{3}{2}B_0\left[\left(\frac{V}{V_0}\right)^{-7/3} - \left(\frac{V}{V_0}\right)^{-5/3}\right]\left\{1 + \frac{3}{4}(B_0' - 4)\left[\left(\frac{V}{V_0}\right)^{-2/3} - 1\right]\right\},$$

(3)

where B_0 and B_0' are the isothermal bulk modulus and its first derivative at zero pressure, and V is the unit-cell volume. The zero-pressure volume V_0 was determined by micro-focused XRD at ambient pressure. Since the methanol–ethanol mixture solidifies above approximately 10 GPa at ambient temperature, only data at pressure below 10 GPa were selected when performing EOS fitting. The values of the bulk modulus extracted in this work for phases A, B, and C were 235(13) GPa, 222(1) GPa, and 171(1) GPa, respectively. The experimental values of B_0 are listed in Table III, together with other values extracted from previous works for comparison. Interestingly, the bulk moduli of phases A and B show a significant increase. This increase in bulk modulus can be explained by the addition of

interstitial nitrogen atoms, which leads to the formation of partial covalent bonds that strengthen the mechanical properties. Thus, nitrogen modification alters the mechanical properties of iron–nickel alloys. Specifically, the atomic radius of N differs greatly from those of Fe and Ni. Under high pressure, N atoms are small enough to enter the three-dimensional metal lattice interstitially, leading to lattice expansion. The distance between Fe/Ni atoms and N atoms in phase A was found to be 2.535 Å, and that in phase B was 2.636 Å. In addition, nitrogen is highly electronegative, which allows it to capture electrons from metals. This results in a positive charge on the metal atoms. Finally, the interatomic distance of the metals is expanded owing to the repulsion force between them. The B_0 value of phase C obtained in our experiment is consistent with previous observations. The reason why phase C is similar to the phase reported previously is that the all-interstitial sites ($2c$, $2b$, $2d$) are the sites available for N atoms at high pressures within the hexagonal structure. The changes in elastic properties of iron–nickel nitrides are mainly due to cation disorder substitution and interstitial nitrogen.

TABLE II. Space group, lattice parameters a and c, and unit-cell volume V of the three phases for iron–nickel nitrides and reference phases.

| Phase	Space group	a (Å)	c (Å)	V (Å³)	Reference
A (γ-FeNi₃ type)					
FeNi₃.₂₁N₀.₀₈	$Pm\bar{3}m$	3.571(9)	...	45.572(2)	This work
FeNi₃	$Pm\bar{3}m$	3.564	...	45.270(2)	43
B (γ-Fe₄N type)					
Fe₂.₉₄Ni₁.₀₈N	$Pm\bar{3}m$	3.773(1)	...	53.711(2)	This work
Fe₄N	$Pm\bar{3}m$	3.7972(1)	...	54.5	42
Fe₃NiN	$Pm\bar{3}m$	3.775(1)	...	53.80	44
C (ε-Fe₃N type)					
Fe₁.₅₈Ni₁.₄₂N	$P6_322$	4.687(1)	4.387(2)	83.472(3)	This work
Fe₃N	$P6_322$	4.660(6)	4.337(5)	81.595(9)	20

TABLE III. Experimental and calculated bulk modulus B_0 and its first derivative B_0' at zero pressure for iron–nickel nitrides.

Phase	Space group	Method[a]	P (GPa)	B_0	B_0'	Reference
A (γ-FeNi$_3$ type)						
FeNi$_{3.21}$N$_{0.08}$	$Pm\bar{3}m$	DAC-SR	0–25	235(13)	4.0	This work
FeNi$_3$	$Pm\bar{3}m$	DFT	. . .	193.7	. . .	43
FeNi$_{0.586}$	$Pm\bar{3}m$	DAC-SR	0–48	160(15)	4.0	45
B (γ-Fe$_4$N type)						
Fe$_{2.94}$Ni$_{1.08}$N	$Pm\bar{3}m$	DAC-SR	0–25	222(1)	4.0	This work
Fe$_4$N	$Pm\bar{3}m$	DAC-SR	0–33	155.8(6)	4.23	46
Fe$_4$N	$Pm\bar{3}m$	DAC-SR	0–31	155(3)	4.0	47
Fe$_4$N	$Pm\bar{3}m$	DFT	. . .	166	4.24	48
Fe$_4$N	$Pm\bar{3}m$	DFT	. . .	191.8	. . .	49
C (ε-Fe$_3$N type)						
Fe$_{1.58}$Ni$_{1.42}$N	$P6_322$	DAC-SR	0–25	171(2)	5.7	This work
Fe$_{2.333}$N	$P6_322$	DAC-SR	0–51	168	5.7	44
Fe$_{2.727}$N	$P6_322$	DAC-SR	0–10	172(4)	5.7	21
Fe$_{3.75}$N	$P6_322$	MA	0–31	162(3)	4.0	50
Fe$_3$N	$P6_322$	DAC-SR	0.8–45.1	154(2)	4.0	24
Fe$_3$N	$P6_322$	DFT	. . .	214	. . .	21
Fe$_3$N	$P6_322$	DFT	. . .	170.9	. . .	51
Fe$_3$N	$P6_322$	DFT	. . .	191.5	. . .	52

[a]MA, multi-anvil press; DAC-SR, diamond anvil cell experiment in synchrotron radiation; DFT, density functional theory.

The Rietveld refinements of NPD patterns acquired from the iron–nickel nitrides are shown in Fig. 6(a). In the NPD refinements, phases A, B, and C and copper were considered. From the refined NPD patterns, copper makes little contribution to the diffraction.

With cation disorder taken into account, the reliability factors of the refinements were found to be the lowest ($R_{wp} = 30.2\%$ and $\chi2 = 2.09$). The R_{wp} factor may be related to the nonstoichiometry, since the nonstoichiometric ratios of transition metal nitrides have an impact
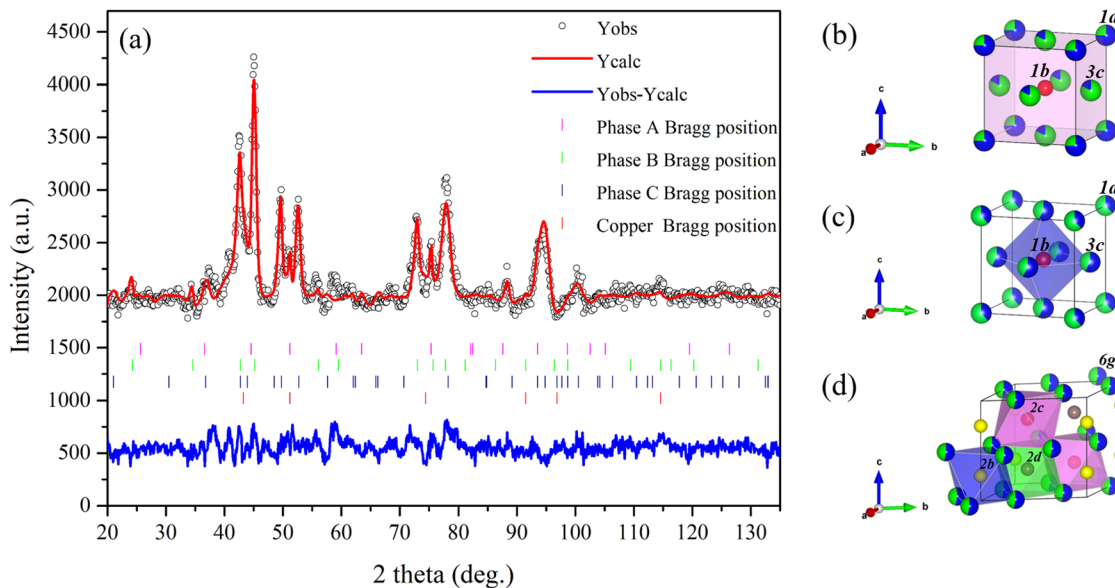
FIG. 6. (a) Rietveld-refined NPD patterns for iron–nickel nitrides. (b), (c), and (d) Crystal structures of three iron–nickel nitrides as determined from NPD refinement, corresponding to phases A, B, and C, respectively. For phases A and B, the Fe and Ni atoms simultaneously occupy the cation sites (3c and 1a), and the N atom occupies the 1b site. For phase C, the Ni atoms partially substitute for Fe atoms at 6g sites, and the N atoms diffuse from 2c (red) to 2b (yellow) and 2d (brown) sites.

on their structural stability.[53] Figure 6(b) shows the crystal structure of phase A. Ni atoms partially substitute for Fe atoms at $1a$ sites, and Fe atoms partially substitute for Ni atoms at $3c$ sites. On the basis of the NPD refinement results, the measured site occupancies of Fe/Ni atoms for $3c$ and $1a$ sites are 0.198/0.801 and 0.750/0.248, respectively (Table IV, phase A). A possible explanation for this is that the $1a$ sites are occupied by Fe and the $3c$ sites by Ni in the ordered L1$_2$ structure, with significant difference with respect to the ordered L1$_2$ structure (L1$_2$ is defined as fcc-based, with different types of atoms at the eight vertices and six face centers). In this work, the measured site occupancies of Fe atoms for $3c$ and $1a$ sites were 0.198 and 0.750, respectively, and the site occupancies of Ni atoms for $3c$ and $1a$ sites were 0.801 and 0.248, respectively. Therefore, phase A should correspond to the completely cation-disordered compound. Meanwhile, the measured $1b$ site occupancy for N atoms is 0.061 (occ.$_{1b}$ = 0.061). As a consequence, interstitial N atoms can still enter the γ-FeNi$_3$-type lattice and form interstitial solid solutions under high pressure.

Previous studies have shown that Ni substitution is beneficial to $1a$ sites in γ-Fe$_4$N.[43] In this work, however, we have shown the possibility of stabilizing a random alloy of Ni atoms on the $1a$ and $3c$ sites, if configurational entropy is considered. In phase B [Fig. 6(c)], Ni atoms partially substitute for Fe atoms at $3c$ sites, Fe atoms partially substitute for Ni atoms at $1a$ sites, and the N atom occupies the $1b$ position. The measured site occupancies of Fe/Ni atoms for $3c$ and $1a$ sites are 0.543/0.455 and 0.378/0.621 (Table IV, phase B). It can be seen here that the disorder of the cations leads to an increase in entropy, with consequent significant improvements in structural stability. Extra stability is also provided by the addition of interstitial nitrogen into phases A and B as compared with the γ-Fe structure.

In addition, Fig. 6(d) shows that Ni atoms partially substitute for Fe atoms at $6g$ sites, and all the voids ($2c$, $2b$, and $2d$ sites) formed by hcp-Fe may be occupied by N atoms in the N-rich phase C (ε-Fe$_3$N type). When these positions are completely occupied, the coordination number of each iron atom is equal to 6 (CN = 6). The measured site occupancies of N atoms for $2c$, $2b$, and $2d$ sites are 0.552, 0.313, and 0.133 according to the Rietveld-refined NPD pattern (Table IV, phase C). As can be seen, the main N site is the $2c$ site, while the $2b$ and

$2d$ positions can also be occupied. We denote Fe atoms with CN = 1, 2, 3, 4, 5, and 6 by Fe(1), Fe(2), Fe(3), Fe(4), Fe(5), and Fe(6), respectively. It has been found that in ε-Fe$_3$N$_{1.098}$ ($P6_322$ structure), the probabilities of occurrence $P^{Fe(0)}$, $P^{Fe(1)}$, $P^{Fe(2)}$, $P^{Fe(3)}$, $P^{Fe(4)}$, $P^{Fe(5)}$, and $P^{Fe(6)}$ are 2.0%, 17.6%, 45.8%, 28.5%, 5.9%, 0.3%, and 0.004%, respectively.[18] We employ a similar notation for phase C, with, for example, Fe/Ni(0) representing an Fe/Ni atom whose N-coordination number (Fe/Ni by N) is 0. Then, $P^{Fe/Ni(0)} \approx 7.5\%$ in phase C, since $P^{Fe/Ni(0)} = (1 - occ._{2c})^2(1 - occ._{2b})^2(1 - occ._{2d})^2$. The values of occ.$_{2c}$, occ.$_{2b}$, and occ.$_{2d}$ are shown in Table IV (phase C). Similarly, $P^{Fe/Ni(1)}$, $P^{Fe/Ni(2)}$, $P^{Fe/Ni(3)}$, $P^{Fe/Ni(4)}$, $P^{Fe/Ni(5)}$, and $P^{Fe/Ni(6)}$ are 27.1%, 36.1%, 22.1%, 6.4%, 0.8%, and 0.038%, respectively. Because $P^{Fe/Ni(0)} > P^{Fe(0)}$ and $P^{Fe/Ni(1)} > P^{Fe(1)}$, the local magnetic moments of iron–nickel nitrides are higher.

On the basis of the Hume-Rothery rules,[54] it is challenging to achieve substitution between Fe and Ni, owing to the difference in atomic size being greater than 15%. In this work, however, Fe and Ni atoms were substituted to form substitutional solid solutions despite the atomic-size difference being as high as 18.25%. However, it can be expected that changes in interatomic distances and interactions under extreme HTHP conditions will lead to broadening of energy bands and allow deep modification of bonding patterns and electronic orbitals. HTHP confinement conditions favor substitutional and interstitial site disordering in ternary iron–nickel nitrides.

IV. CONCLUSION

In summary, novel spherical bulk iron–nickel nitrides were successfully synthesized through an HPSSM reaction under a pressure of 5 GPa and a temperature of 1673 K. The structural properties of the as-prepared samples were fully characterized by NPD, SEM, HAADF-STEM, SAED, micro-focus XRD, and synchrotron radiation ADXRD. The obtained spherical-like bulk samples were found to include three N-bearing compounds (γ-FeNi$_3$ type, γ-Fe$_4$N type, and ε-Fe$_3$N type) owing to dendrite segregation of the nickel-based alloy. The crystal structure and site occupation of each phase were analyzed and discussed in detail. The Fe and Ni atoms were found to occupy the lattice positions in a disorderly manner. These significant elastic properties can be attributed to the joint action of interstitial N atoms and disorderly substituted Ni atoms.

DATA AVAILABILITY

The data that support the findings of this study are available from the corresponding authors upon reasonable request.

REFERENCES

[1]F. Brich, "Elasticity and constitution of the Earth's interior," J. Geophys. Res. **57**, 227–286, https://doi.org/10.1029/JZ057i002p00227 (1952).

[2]F. Brich, "Density and composition of mantle and core," J. Geophys. Res. **69**, 4377–4388, https://doi.org/10.1029/JZ069i020p04377 (1964).

TABLE IV. Structural information on the three phases within iron–nickel nitrides obtained from the Rietveld-refined NPD patterns, with R_{wp} = 30.2% and χ^2 = 2.09.

	Atom	Wyckoff	x	y	z	Occ.
Phase A	Fe	$1a$	0	0	0	0.750(7)
		$3c$	0	1/2	1/2	0.198(1)
	Ni	$1a$	0	0	0	0.248(6)
		$3c$	0	1/2	1/2	0.801(6)
	N	$1b$	1/2	1/2	1/2	0.061(4)
Phase B	Fe	$1a$	0	0	0	0.378(7)
		$3c$	0	1/2	1/2	0.543(5)
	Ni	$1a$	0	0	0	0.621(6)
		$3c$	0	1/2	1/2	0.455(3)
	N	$1b$	1/2	1/2	1/2	0.920(1)
Phase C	Fe	$6g$	0.3278	0	0	0.525(3)
	Ni	$6g$	0.3278	0	0	0.473(1)
	N	$2c$	1/3	2/3	1/4	0.552(9)
	N	$2b$	0	0	1/4	0.313(8)
	N	$2d$	2/3	1/3	1/4	0.133(2)

[3]O. L. Anderson, "The Earth's core and the phase diagram of iron," Philos. Trans. R. Soc. London, Ser. A **306**, 21–35 (1982).

[4]A. Jephcoat and P. Olson, "Is the inner core of the Earth pure iron?," Nature **325**, 332–335 (1987).

[5]K. D. Litasov, A. Shatskiy, D. S. Ponomarev, and P. N. Gavryushkin, "Equations of state of iron nitrides ε-Fe$_3$N$_x$ and γ-Fe$_4$N$_y$ to 30 GPa and 1200 K and implication for nitrogen in the Earth's core," J. Geophys. Res. **122**, 3574–3584, https://doi.org/10.1002/2017jb014059 (2017).

[6]T. Takahashi, W. A. Bassett, and H.-K. Mao, "Isothermal compression of the alloys of iron up to 300 kilobars at room temperature: Iron–nickel alloys," J. Geophys. Res. **73**, 4717–4725, https://doi.org/10.1029/jb073i014p04717 (1968).

[7]E. Huang, W. A. Bassett, and M. S. Weathers, "Phase relationships in Fe-Ni alloys at high pressures and temperatures," J. Geophys. Res. **93**, 7741–7746, https://doi.org/10.1029/jb093ib07p07741 (1988).

[8]H. K. Mao, Y. Wu, L. C. Chen, J. F. Shu, and A. P. Jephcoat, "Static compression of iron to 300 GPa and Fe$_{0.8}$Ni$_{0.2}$ alloy to 260 GPa: Implications for composition of the core," J. Geophys. Res. **95**, 21737–21742, https://doi.org/10.1029/jb095ib13p21737 (1990).

[9]R. J. Hemley and H. K. Mao, "In situ studies of iron under pressure: New windows on the Earth's core," Int. Geol. Rev. **43**, 1–30 (2001).

[10]X. G. Diao, A. Y. Takeuchi, F. Garcia, R. B. Scorzelli, and H. R. Rechenberg, "Magnetic properties of perovskite-type Fe–Ni nitrides γ'-(Fe$_{1-x}$Ni$_x$)$_4$N ($0 \leqslant x \leqslant 0.9$)," J. Appl. Phys. **85**, 4485–4487 (1999).

[11]M. Schilfgaarde, I. A. Abrikosov, and B. Johansson, "Origin of the Invar effect in iron–nickel alloys," Nature **400**, 46–49 (1999).

[12]Y. Himuro, Y. Tanaka, I. Ohnuma, R. Kainuma, and K. Ishida, "Phase equilibria and γ'-L1$_2$ phase stability in the Ni-rich portion of Ni–Fe–Si and Ni–Fe–Al systems," Intermetallics **13**, 620–630 (2005).

[13]X. Wang, W. T. Zheng, H. W. Tian, S. S. Yu, W. Xu, S. H. Meng, X. D. He, J. C. Han, C. Q. Sun, and B. K. Tay, "Growth, structural, and magnetic properties of iron nitride thin films deposited by dc magnetron sputtering," Appl. Surf. Sci. **220**, 30–39 (2003).

[14]H. J. Grabke, "The role of nitrogen in the corrosion of iron and steels," ISIJ Int. **36**, 777–786 (1996).

[15]A. Morisako, M. Matsumoto, and M. Naoe, "Magnetic anisotropy and soft magnetism of iron nitride thin films prepared by facing-target sputtering," J. Appl. Phys. **69**, 5619–5621 (1991).

[16]B. C. Frazer, "Magnetic structure of Fe$_4$N," Phys. Rev. **112**, 751–754 (1958).

[17]A. Leineweber, H. Jacobs, F. Hüning, H. Lueken, H. Schilder, and W. Kockelmann, "ε-Fe$_3$N: Magnetic structure, magnetization and temperature dependent disorder of nitrogen," J. Alloys Compd. **288**, 79–87 (1999).

[18]W. W. George and J. A. Berger, "Structure and magnetic properties of some transition metal nitrides," J. Met. **7**, 360–368 (1955).

[19]R. N. Panda and N. S. Gajbhiye, Magnetic properties of nanocrystalline γ–Fe–Ni–N nitride systems, J. Appl. Phys **86**(6), 3295–3302 (1990).

[20]L. Lei, L. Zhang, S. Gao, Q. Hu, L. Fang, X. Chen, Y. Xia, X. Wang, H. Ohfuji, Y. Kojima, S. A. T. Redfern, Z. Zeng, B. Chen, D. He, and T. Irifune, "Neutron diffraction study of the structural and magnetic properties of ε-Fe$_3$N$_{1.098}$ and ε-Fe$_{2.322}$Co$_{0.678}$N$_{0.888}$," J. Alloys Compd. **752**, 99–105 (2018).

[21]R. Niewa, D. Rau, A. Wosylus, K. Meier, M. Hanfland, M. Wessel, R. Dronskowski, D. A. Dzivenko, R. Riedel, and U. Schwarz, "High-pressure, high-temperature single-crystal growth, ab initio electronic structure calculations, and equation of state of ε-Fe$_3$N$_{1+x}$," Chem. Mater. **21**, 392–398 (2009).

[22]K. Guo, D. Rau, L. Toffoletti, C. Müller, U. Burkhardt, W. Schnelle, R. Niewa, and U. Schwarz, "Ternary metastable nitrides ε-Fe$_2$TMN (TM = Co, Ni): High-pressure, high-temperature synthesis, crystal structure, thermal stability, and magnetic properties," Chem. Mater. **24**, 4600–4606 (2012).

[23]L. Lei and L. Zhang, "Recent advance in high-pressure solid-state metathesis reactions," Matter Radiat. Extremes **3**, 95–103 (2018).

[24]W. Yin, L. Lei, X. Jiang, P. Liu, F. Liu, Y. Li, F. Peng, and D. He, "High pressure synthesis and properties studies on spherical bulk ε-Fe$_3$N," High Pressure Res. **34**, 317–326 (2014).

[25]L. Zhang, S. Gao, Q. Hu, L. Qi, L. Feng, and L. Lei, "Synthesis and characterization of spherical-like bulk ε-Fe$_{3-x}$Co$_x$N (x = 0.0, 0.25, 1.95)," Mater. Chem. Phys. **197**, 94–99 (2017).

[26]L. Qi, L. Lei, Q. Hu, L. Zhang, L. Feng, M. Pu, H. Ohfuji, and T. Irifune, "Strengthening effects of interstitial nitrogen on rhenium," J. Appl. Phys. **123**, 055911 (2018).

[27]X. Jiang, L. Lei, Q. Hu, Z. C. Feng, and D. He, "High-pressure Raman spectroscopy of Re$_3$N crystals," Solid State Commun. **201**, 107–110 (2015).

[28]S. Wang, H. Ge, S. Sun, J. Zhang, F. Liu, X. Wen, X. Yu, L. Wang, Y. Zhang, H. Xu, J. C. Neuefeind, Z. Qin, C. Chen, C. Jin, Y. Li, D. He, and Y. Zhao, "A new molybdenum nitride catalyst with rhombohedral MoS$_2$ structure for hydrogenation applications," J. Am. Chem. Soc. **137**, 4815–4822 (2015).

[29]Choong-Shik Yoo, "Chemistry under extreme conditions: Pressure evolution of chemical bonding and structure in dense solids," Matter Radiat. Extremes **5**(018202), (2020), 018202-1-018202-14.

[30]H. Ohfuji and M. Yamamoto, "EDS quantification of light elements using osmium surface coating," J. Miner. Petrol. Sci. **110**, 189–195 (2015).

[31]H. K. Mao, J. Xu, and P. M. Bell, "Calibration of the ruby pressure gauge to 800 kbar under quasi-hydrostatic conditions," J. Geophys. Res. **91**, 4673–4676, https://doi.org/10.1029/jb091ib05p04673 (1986).

[32]A. P. Hammersley, S. O. Svensson, M. Hanfland, A. N. Fitch, and D. Hausermann, "Two-dimensional detector software: From real detector to idealised image or two-theta scan," High Pressure Res. **14**, 235 (1996).

[33]N. Hirao, S. I. Kawaguchi, K. Hirose, K. Shimizu, E. Ohtani and Y. Ohishi"New developments in high-pressure X-ray diffraction beamline for diamond anvil cell at SPring-8, Matter Radiat. Extremes, 5(018403) (2020) 018403-1-018403-10.

[34]J. Rodriguez-Carvajal, An Introduction to the Program FullProf 2000 (Laboratoire Le ón Brillouin, CEA-CNRS: Saclay, France, 2001).

[35]K. B. Zhang, Z. Y. Fu, J. Y. Zhang, J. Shi, W. M. Wang, H. Wang, Y. C. Wang, and Q. J. Zhang, "Annealing on the structure and properties evolution of the CoCrFeNiCuAl high-entropy alloy," J. Alloys Compd. **502**, 295–299 (2010).

[36]A. Epishin, T. Link, U. Brückner, B. Fedelich, and P. Portella, "Effects of segregation in nickel-base superalloys: Dendritic stresses," Superalloys, 537–543 (2004).

[37]L. Lei and D. He, "Synthesis of GaN crystals through solid-state metathesis reaction under high pressure," Cryst. Growth Des. **9**, 1264–1266 (2009).

[38]L. Lei, W. Yin, X. Jiang, S. Lin, and D. He, "Synthetic route to metal nitrides: High-pressure solid-state metathesis reaction," Inorg. Chem. **52**, 13356–13362 (2013).

[39]L. Xie, X. Chen, L. Fang, G. Sun, C. Xie, B. Chen, H. Li, V. A. Ulyanov, V. A. Solovei, M. R. Kolkhidashvili, A. P. Bulkin, S. I. Kalinin, Y. Wang, and X. Wang, "Fenghuang: High-intensity multi-section neutron powder diffractometer at CMRR," Nucl. Instrum. Methods Phys. Res., Sect. A **915**, 31–35 (2019).

[40]Q. Hu, L. Fang, Q. Li, X. Li, X. Chen, L. Xie, J. Zhang, F. Liu, L. Lei, G. Sun, and D. He, "Enhancing the pressure limitation in large-volume Bridgman-anvil cell used for in situ neutron diffraction," High Pressure Res. **39**, 655–665 (2019).

[41]L.-h. Feng, Q.-w. Hu, L. Lei, L.-m. Fang, L. Qi, L.-l. Zhang, M.-f. Pu, Z.-l. Kou, F. Peng, X.-p. Chen, Y.-h. Xia, Y. Kojima, H. Ohfuji, D.-w. He, B. Chen, and T. Irifune, "Neutron powder diffraction and high-pressure synchrotron x-ray diffraction study of tantalum nitrides," Chin. Phys. B **27**, 026201 (2018).

[42]A. Takeuchi and A. Inoue, "Classification of bulk metallic glasses by atomic size difference, heat of mixing and period of constituent elements and its application to characterization of the main alloying element," Mater. Trans. **46**, 2817–2829 (2005).

[43]G. Wang, Q. Hu, K. Kokko, B. Johansson, and L. Vitos, "Ab initio investigation of the elastic properties of Ni$_3$Fe," Phys. Rev. B **88**, 174205 (2013).

[44]P. Monachesi, T. Björkman, T. Gasche, and O. Eriksson, "Electronic structure and magnetic properties of Mn, Co, and Ni substitution of Fe in Fe$_4$N," Phys. Rev. B **88**, 054401 (2013).

[45]E. Huang, W. A. Bassett, and M. S. Weathers, "Phase diagram and elastic properties of Fe30%Ni alloy by synchrotron radiation," J. Geophys. Res. **97**, 4497–4502, https://doi.org/10.1029/92JB00020 (1992).

[46]K. Guo, D. Rau, J. von Appen, Y. Prots, W. Schnelle, R. Dronskowski, R. Niewa, and U. Schwarz, "High pressure high-temperature behavior and magnetic properties of Fe$_4$N: Experiment and theory," High Pressure Res. **33**, 684–696 (2013).

[47]J. F. Adler and Q. Williams, "A high-pressure X-ray diffraction study of iron nitrides: Implications for Earth's core," J. Geophys. Res. **110**, B01203, https://doi.org/10.1029/2004jb003103 (2005).

[48]R. Niewa, D. Rau, A. Wosylus, K. Meier, M. Wessel, M. Hanfland, R. Dronskowski, and U. Schwarz, "High-pressure high-temperature phase transition of γ'-Fe$_4$N," J. Alloys Compd. **480**, 76–80 (2009).

[49]T. Gressmann, M. Wohlschlögel, S. Shang, U. Welzel, A. Leineweber, E. J. Mittemeijer, and Z.-K. Liu, "Elastic anisotropy of γ'-Fe$_4$N and elastic grain

interaction in γ'-Fe$_4$N$_{1-y}$ layers on α-Fe: First-principles calculations and diffraction stress measurements," Acta Mater. **55**, 5833–5843 (2007).

[50] K. D. Litasov, A. F. Shatskiy, S. G. Ovchinnikov, Z. I. Popov, D. S. Ponomarev, and E. Ohtani, "Phase transformations of Fe$_3$N-Fe$_4$N iron nitrides at pressures up to 30 GPa studied by *in situ* X-ray diffractometry," JETP Lett. **98**, 805–808 (2014).

[51] W. H. Zhang, Z. Q. Lv, Z. P. Shi, S. H. Sun, Z. H. Wang, and W. T. Fu, "Electronic, magnetic and elastic properties of ε-phases Fe$_3$X(X=B, C, N) from density-functional theory calculations," J. Magn. Magn. Mater. **324**, 2271–2276 (2012).

[52] Y.-J. Shi, Y.-L. Du, and G. Chen, "First-principles study on the elastic and electronic properties of hexagonal ε-Fe$_3$N," Comput. Mater. Sci. **67**, 341–345 (2013).

[53] S. Wang, X. Yu, J. Zhang, M. Chen, J. Zhu, L. Wang, D. He, Z. Lin, R. Zhang, K. Leinenweber, and Y. Zhao, "Experimental invalidation of phase-transition-induced elastic softening in CrN," Phys. Rev. B **86**, 064111 (2012).

[54] M.-x. Ren, B.-s. Li, and H.-z. Fu, "Formation condition of solid solution type high-entropy alloy," Trans. Nonferrous Met. Soc. China **23**, 991–995 (2013).